HETEROTYPIC ENDOSOMAL INTERACTIONS DRIVE EMERGENT EARLY ENDOSOMAL MATURATIONS

Harrison M York[1] * †, Kunaal Joshi[2] †, Charles S Wright[2] †, Ullhas K Moorthi[1], Hetvi Gandhi[1], Abhishek Patil[1], Srividya Iyer-Biswas[2,3] * and Senthil Arumugam[1,4,5] *

† Equal contributions

[1]Monash Biomedicine Discovery Institute, Faculty of Medicine, Nursing and Health Sciences, Monash University, Clayton/Melbourne, VIC 3800, Australia
[2]Department of Physics and Astronomy, Purdue University, West Lafayette, IN 47907, USA
[3]Santa Fe Institute, Santa Fe, NM 87501, USA
[4]ARC Centre of Excellence in Advanced Molecular Imaging, Monash University, Clayton/ Melbourne, VIC 3800, Australia
[5]Single Molecule Science, European Molecular Biological Laboratory Australia (EMBL Australia), University of New South Wales, Sydney, Australia.

*Correspondence: harrison.york@monash.edu, iyerbiswas@purdue.edu and senthil.arumugam@monash.edu

ABSTRACT

Endosomal trafficking in single cells entails the generation of membrane vesicles; their motor protein-mediated transport; morphological alterations such as tubulation, fusion and fission; as well as dynamic maintenance of various identities, defined by the lipid composition and localisation of specific proteins on their membranes. Endosomal maturation is a major feature of this process. It is classically described as endosomes shedding one specific protein and acquiring another, resulting in an identity change. This step governs the flux and the number of distinct endosomal populations. Many of the molecular players that characterise different compartments have been identified—for example, APPL1 on very early endosomes, and EEA1 on early endosomes. However, *how* an ensemble population of endosomes matures at a *whole cell level* has remained unstudied. Here, we describe a novel inter-endosomal interaction-based feed-forward mechanism that drives endosomal conversions and controls ensemble conversion rates at the whole cell level. Furthermore, using live-cell Förster Resonance Energy Transfer, we demonstrate that this process is underpinned by co-ordinated precedence in EEA1 binding via its N- and C-terminal domains, ensuring the biochemical maturation of these vesicles. Using simulations, we provide a quantitative framework to recapture the experimentally observed characteristics in the reaction scheme and the activity of EEA1. We demonstrate that the model of APPL1 to EEA1 endosomal maturation needs to be extended to include heterotypic interactions between endosomes that result in conversions, which form a significant fraction of events, in addition to the previously reported single endosome-centric maturation models. Based on these results, we motivate how temporal specificity emerges in an inherently stochastic system—namely, through a timekeeping mechanism via an N-terminal EEA1 trigger that enables deterministic outcomes in ensemble endosomal conversions.

INTRODUCTION

A hallmark of eukaryotic cells is compartmentalisation through membranous organelles. This strategy enables the spatial separation of cellular components and the maintenance of distinct reaction environments, with critical functionality provided by selective interactions between and dynamic localisation of these organelles. To control these processes, cells have evolved a highly complex intracellular trafficking network that is governed by the external presentation of each membrane compartment. Each membrane has a unique 'character' defined by the presence of key membrane proteins such as Rab-family GTPases, signalling lipids including phosphoinositides, and effector proteins, which together control the interaction of the compartment with the intracellular environment.

Following formation at the plasma membrane via endocytosis, endosomes undergo maturation processes [1] brought about by the concerted effects of motility (driven by motor proteins), inter-endosomal fusions, fissions (resulting from tubulation), and endosomal conversions. Conversions are switch-like processes in which endosomes shed one specific set of proteins and acquire another [2, 3]. In concert with protein conversions are phosphoinositide conversions, with specific phosphoinositide species constituting the modules of coincidence detection mechanisms exhibited by various proteins. Thus, phosphoinositide species provide a second layer of regulation, governing which proteins will be localised to a specific subset of endosomes [4, 5].

The individual processes that constitute the ensemble 'conveyor belt' of endosomal maturation—including motility, lipid conversion and binding/unbinding of proteins—are inherently stochastic. Furthermore, newly generated endosomes are relatively smaller in size; thus, stochasticity is expected to play an important role. Our current understanding of the dynamics of endosomal maturations, especially that of adaptor protein, phosphotyrosine interacting with PH domain and leucine zipper 1 (APPL1) to early endosomal antigen 1 (EEA1), comes from live cell imaging, which was limited in achieving whole-cell volumetric imaging with sufficient temporal resolution. This lack of rapid volumetric imaging precludes the measurement of all events, including inter-endosomal interactions, which would be necessary to enable absolute quantification to describe a complete picture. However, these seminal studies did capture the process of individual endosomes undergoing direct conversions [2, 3]. A description of individual endosomes undergoing conversions has led to a single endosome-centric model, wherein a phosphoinositide switch controls the transition from APPL1 to EEA1 on an individual endosome [3]. APPL1 and EEA1 bind to endosomes via coincidence detection binding to Rab5, as well as the phosphoinositides PI(3,4)P2 and PI(3)P, respectively. In accordance with this, inducible depletion of PI(3)P has been shown to result in a reverse EEA1 to APPL1 conversion, leading Zoncu et al. to suggest that APPL1 to EEA1 maturation is underpinned by this phosphoinositide switch. PI(3,4)P2 can be dephosphorylated into PI(3)P by two phosphoinositide 4-phosphatases in mammals, INPP4A and INPP4B [6, 7] . These two isoforms show highly variable expression levels across different tissues and have been suggested to localise to distinct intracellular localisations, with INPP4A being found on Rab5-positive endosomes [8, 9].

However, key questions remain: What triggers the phosphoinositide switch? How do populations of endosomes mature? How many conversions take place? Vesicle fusions are abundant in the very early to early endosomal populations, leading to the mixing of cargo,

lipids and endosomal proteins. Such inter-endosomal interactions including fusions and 'kiss-and-run' events have been implicated in endosome to lysosome delivery of cargo [10] and in endosomes and phagosomes [11]; however, how the processes of fusions and conversions intercalate in endosomal maturations remains largely unstudied. To date, no whole cell measurements have been performed to measure ensemble endosomal conversions. Due to the highly stochastic nature of this system, dynamic measurements of the complete set of relevant events are essential to construct an accurate mechanistic description. Stochasticity poses crucial challenges in maintaining causal ordering and temporal specificity, i.e., a tight probability distribution of events in time. For thresholded or first-passage processes [12], such as those considered here, the effect can be characterised through the width of the first-passage time distribution [13]. Despite the emphasis on stochasticity in constituent dynamics in the vesicular transport system [14], endosomal trafficking processes display an extraordinary degree of robustness and predictability in delivering cargo to specific intracellular destinations. Analogously, receptors known to be transported through the endosomal system show reproducible signalling outcomes. These properties suggest that there exist mechanisms to counter the stochasticity of the constituent processes and thus to achieve tight control over maturation, trafficking and dynamics of the intracellular transport system.

Here, we used lattice light-sheet microscopy (LLSM) live-cell imaging of APPL1 and EEA1, which allows rapid imaging of whole cell volumes for extended periods of time [15]. To quantify these data, we developed a bespoke endosome detection and tracking algorithm to detect large numbers of endosomal collisions, fusions and conversions occurring within many single cells over a prolonged period of imaging. We complemented these methods with live-cell fluorescence lifetime microscopy (FLIM) to interrogate the molecular orientation of EEA1, a head-to-head homodimer bound to maturing early endosomes. We show that very early endosome (VEE) to early endosome (EE) conversion is a multistep process, underpinned by the multiple asymmetric binding sites of EEA1 and its cyclical conformation changes, which is brought about by endosomal collisions and heterotypic fusions. Through simulations, we test the effectiveness of our proposed mechanism in predicting the maturation time course, specifically conversion from APPL1 to EEA1 and from N- to C-terminal EEA1 attachments. The new details warrant a significant upgrade to the model of endosomal maturations, with heterotypic interactions—where collisions lead to triggered conversions or fusions—forming a large fraction of events leading to endosomal maturations. Furthermore, our simulations indicate that this emergent mechanism imparts tight temporal control over the ensemble maturation of VEEs.

RESULTS

To simultaneously measure ensemble endosomal conversion dynamics, and also follow individual endosomes at whole cell levels with fast spatio-temporal resolution, we used lattice light-sheet microscopy (LLSM) to image cells expressing APPL1-EGFP [16] and TagRFP-T EEA1 [17]. LLSM-based live-cell imaging enabled near-diffraction limited prolonged imaging of ~30 minutes with a temporal resolution of ~3 seconds per entire volume of the cell with minimal photobleaching (Figure 1a, Supplementary Movie 1). Rapid LLSM imaging confirmed minimal overlap between APPL1 and EEA1 signals with the exception of rapid switch-like APPL1 to EEA1 conversions (Figure 1b), as has been reported previously [3]. Visual inspection of the data revealed three major categories of dynamic phenomenologies: inter-

endosomal ‘kiss-and-run’ events preceding conversions, inter-endosomal collisions leading to fusion, and conversions (Figure 2a, Supplementary Movie 1, 2).

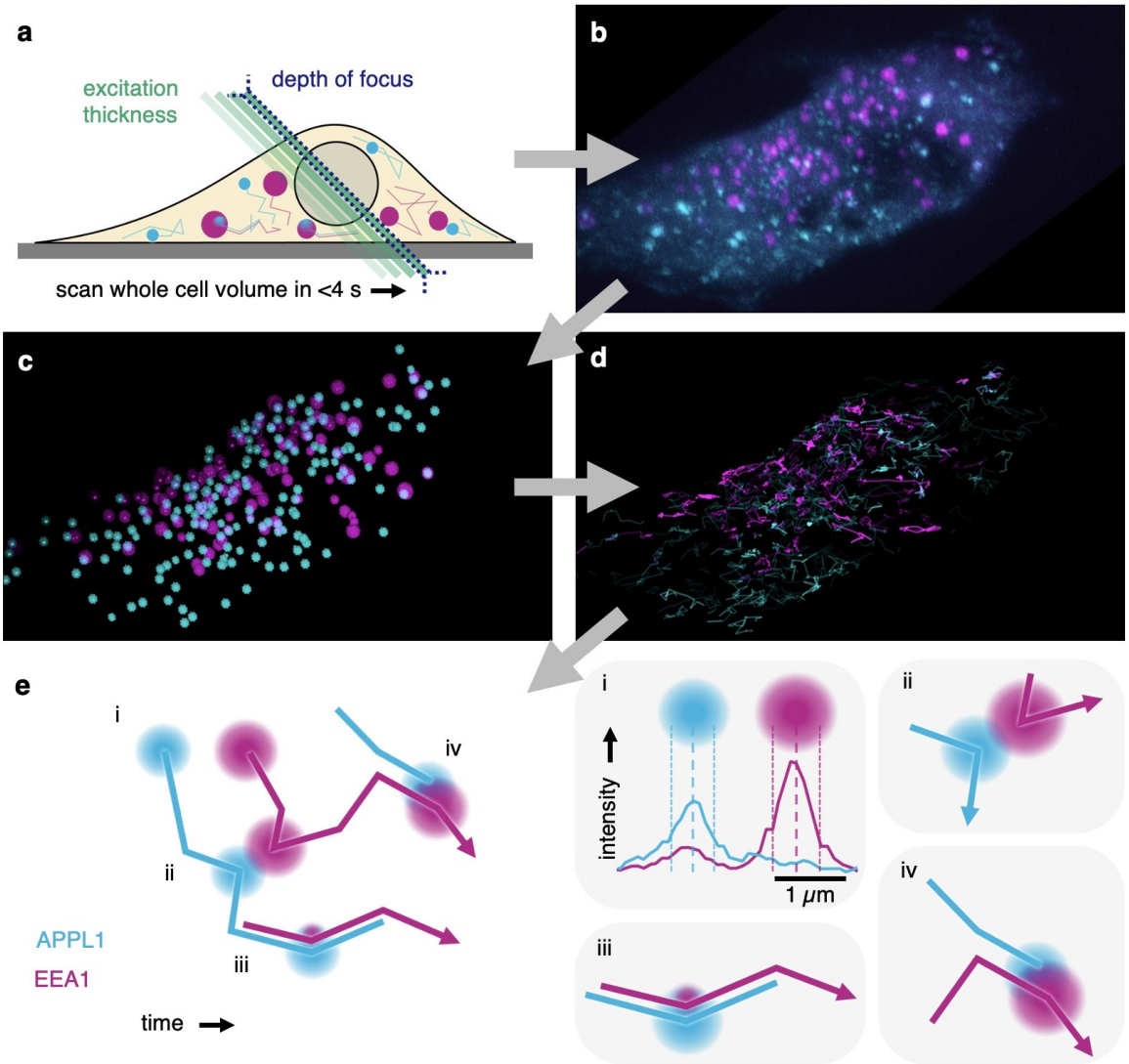

Figure 1. Image analysis pipeline to measure ensemble endosome characteristics. Representative images of each stage of imaging workflow used to detect and measure endosomes at a whole cell level. **a)** APPL1-EGFP and EEA1-T-TagRFP are imaged using LLSM at 2.5 seconds/volume, yielding **b)** whole cell volumes lasting up to ~30 minutes. **c)** Preliminary endosomes in each channel are identified separately by blob detection then an unsupervised pattern recognition-based routine is used to identify true endosomes, following by **d)** linking based on localisation and intensity values to construct complete trajectories with continuous spatial data and intensity traces. **e)** Trajectories of endosomes identified from opposite channels are then analysed together to identify of events of interest. (i) The intensity profile between two endosomes (*cyan*: APPL1, *magenta*: EEA1) along the line connecting their centres of mass is shown. Dashed line indicates centre of mass; dotted lines indicate endosome boundaries determined by detection routine. Changes in surface–to–surface distances between pairs of nearby events are used to identify events, with (ii) collisions defined as the point of nearest approach, if below the threshold for surface–to–surface separation and (iii) conversions calculated by identifying regions of colocalised trajectories; (iv) such events are considered to be fusions if the EEA1 track that remains after the disappearance of the APPL1 track existed as a distinct tracked object prior to the colocalisation event.

The number of distinct events, and their highly stochastic nature, preclude interpretations based on human-biased selection of representative trajectories. We therefore developed an automated image analysis pipeline to convert raw data to full trajectories of detected endosomes, automatically annotated for the presence of events such as heterotypic collisions, conversions, and fusions. Briefly, we identify all potential endosomes using a blob detection routine (Laplacian of Gaussian operator), then filter to the true endosomes with an unsupervised pattern recognition-based routine (Figure 1c). The brightest and dimmest objects (>100 total) are taken to represent true versus false endosomes, respectively, then used as inputs for template matching to construct a set of features for each class, followed by *k*-means clustering into signal versus background. These discrete segmented objects were then tracked using a custom tracking routine built with trackpy [18], using both localisation and intensity values (Figure 1d, Supplementary Movie 2). Tracked objects from opposite channels are then analysed independently to identify collision, fusion and conversion events based on the time course of spatial separation between nearby endosomes (Figure 1e).

To investigate whether heterotypic interactions play a regulatory role in very early endosomal maturation, we applied this analysis pipeline to six untreated and two nocodazole-treated whole cell volumes (equivalent to >1 hour of total observations), which resulted in detection of thousands of putative events. A representative montage of a conversion preceded by multiple collision events is shown in Figure 2a, with the corresponding intensity trace (with annotated events) in Figure 2b. We applied stringent selection criteria to all automatically identified events to select only clear cases of APPL1–EEA1 conversion (Supplementary Figure 2, Supplementary Movie 3), confirmed by visualisation of population-average signals of APPL1 and EEA1 immediately before, during, and after each conversion event (Figure 2c). During the process of conversion, APPL1 and EEA1 signals for the same endosome showed average colocalisation for ~30 s (Figure 2c), but with considerable variability. This is demonstrated by separating all events into cohorts defined by the total duration of APPL1–EEA1 colocalisation (in bins of 10 s); population averages for each cohort are shown in Figure 2d. During visual inspection of these data, we noticed a clear association between the speed of individual APPL1 to EEA1 conversions and the number of preceding heterotypic collisions. To confirm this observation, we calculated the number of collisions occurring between each APPL1 endosome and any EEA1 endosomes in the 30 s immediately prior to a detected conversion or fusion event, then segmented the distribution of events from each colocalisation cohort according to the number of preceding heterotypic collisions (Figure 2e). Importantly, all slow detected APPL1 to EEA1 conversions and fusions had few or no potential collisions prior to conversion. The relative numbers of each type of event (collision-induced or unaided, fusion or conversion) are summarised in Figure 2f. In line with previous models of EEA1 mediated fusion [19, 20], 39% of the events displayed immediate fusion following collisions ('unaided fusions'). This could be attributed to EEA1-mediated fusion where EEA1 molecules can bridge two endosomes at the instant of collision, as has been postulated previously [19, 21-23]. 38% of events involved fusions, but that were preceded by at least one heterotypic collision ('collision-induced fusions'). While 12% of events represented unaided conversions, which have been reported earlier, collisions leading to conversions were found to be 11% of all events. Together, these events form the endosomal maturation process. Note that heterotypic fusions result in endosomes with both APPL1 and EEA1 and represent an intermediate step in conversion *(vide infra)*. The quantitative analysis also revealed that unaided conversions were more prominent for larger endosomes (Figure 2g), whereas the heterotypic collisions were a feature of a much broader and smaller size of endosomes that showed stochastic

directed runs and transitions to periods of little movement, as has been reported for early endosomes [24]. These results underline the necessity of rapid volumetric imaging and bespoke analysis routines to capture the described processes.

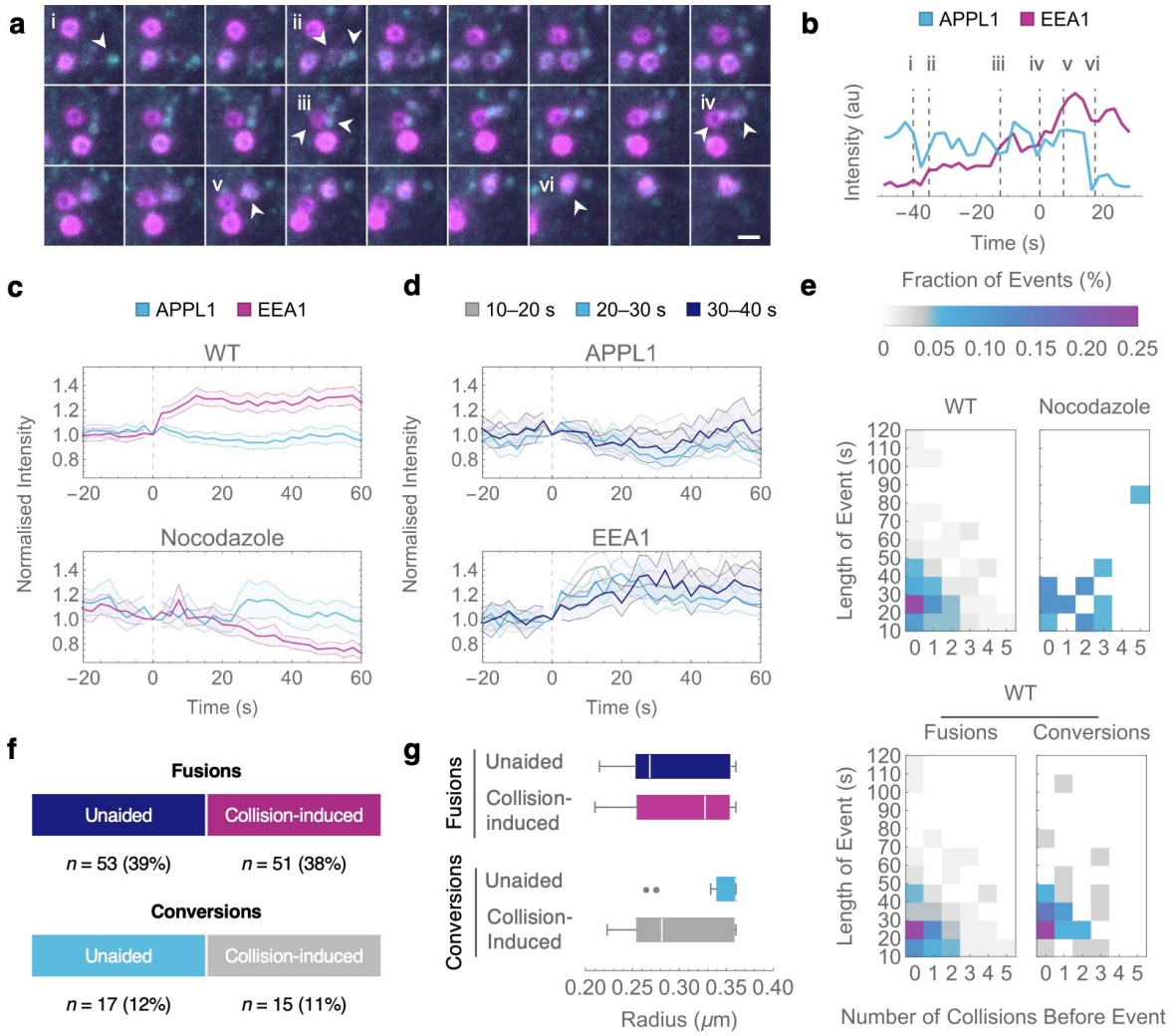

Figure 2. Heterotypic APPL1–EEA1 collisions play a causal role in early endosomal maturation. **a)** Montage showing (i) a single APPL1 endosome that collides with (ii) a dim EEA1 endosome and separates, then collides with (iii) a brighter EEA1 endosome and separates, (iv) collides again with the same EEA1 endosome then (v) separates, at which point EEA1 levels are significantly elevated; by (vi) APPL1 is no longer independently detected. Scale bar = 1 μm. **b)** Corresponding intensity traces with events indicated by dotted vertical lines. Time is reported relative to the start of APPL1–EEA1 colocalisation; intensity is reported as the average value of each channel's intensity over the pixels detected by APPL1 detection until the end of localisation, by EEA1 detection thereafter. **c)** Population-average intensity traces for wild-type (WT) (*top*) and nocodazole-treated (*bottom*) cells, aligned with the start of each conversion event. WT cells demonstrate a steady increase in EEA1 signal and decrease in APPL1 signal from the start of colocalisation, whereas nocodazole-treated cells show no clear separation between the channels, on average (i.e., detected events likely represent 'conversions' that subsequently revert). Up until the end of colocalisation, average intensity was calculated using the mask of the object detected in the APPL1 channel; afterward, it was calculated using the mask of the object detected in the EEA1 channel. Intensity as normalised by the value at the start of detected colocalisation. WT data represent >100 events; nocodazole-treated data represent >25 events; error range shows 95% confidence interval. **d)** Average intensity traces for WT cells, separated into cohorts according to duration of conversion—short (10–20 s), medium (20–30 s), and long (30–40 s)—for APPL1 (*top*) and EEA1 (*bottom*) channels. **e)** Heatmap of the fraction of events that fall into cohorts defined by the total duration of colocalisation (in 10-s bins) and the number of heterotypic collisions

immediately preceding the event. (*Top*) All events are shown for WT (*left*) and nocodazole-treated (*right*) cells. (*Bottom*) WT data are split according to fusions (*left*) and conversions (*right*). Importantly, in WT cells, longer durations of colocalisation are notably less frequent in those cases where multiple collisions occur. Note that nocodazole events represent fusions only, as no conversions were detected for these cells. Total events for each condition are WT (n = 127), which is further segmented into fusions (n = 96) and conversions (n = 32), and nocodazole-treated (n = 18). **f)** Numbers of events observed in each category: unaided fusions (39%), collision-induced fusions (38%), unaided conversions (12%), and collision-induced conversions (11%). Strict criteria were applied to filter the collisions; thus, we consider the values reported here for collision-induced events to likely represent a conservative estimate. **g)** Size distributions of populations of APPL1 endosomes, segmented into four types of events. Endosomes that undergo unaided (direct) conversions are, on average, larger than those that undergo collision-induced conversions or fusions.

Next, to assess whether collisions have a causal effect on early endosomal maturation, we inhibited the motility of the endosomes by abrogating microtubule-associated active transport, through mild nocodazole depolymerisation of microtubules. Visual inspection revealed a drastic effect on the number of conversion events in contrast to uninhibited cells, which was corroborated by automated analysis; population-averaged complete trajectories showed no sustained difference in APPL1 and EEA1 signals after putative conversion events (Figure 2c) and no trend was observed between duration of putative events and number of preceding collisions (Figure 2e, top right). Further, we observed that in nocodazole-treated cells, some endosomes showed vacillating 'back-and-forth' fluctuations between the signals of APPL1 and EEA1, never fully committing to a complete conversion into an EEA1 positive endosome that did not revert (Supplementary Movie 4). Interestingly, a few endosomes displaying EEA1 fluctuations were also ‘pulsatile’ suggesting existence of clustering (Supplementary Figure 3), non-linearity and binding-unbinding events that corresponded to more than a few molecules. Many endosomal markers and associated proteins including dynein have been reported to exist as clusters on the endosomal surface [25-28]. Further, phosphoinositide lipids also display clustering induced by binding of specific proteins [29]. Therefore, we reasoned that, given the observed dynamics, APPL1 and EEA1 may display some level of clustering.

To confirm the existence of clusters of EEA1, we performed single molecule localisation microscopy using EEA1 Dendra-2 [30]. We found that EEA1 was not uniformly distributed over the entire surface of the endosomes, but instead formed distinct domains (Figure 3a). To confirm this observation in live cells and to investigate the distribution of EEA1 with respect to APPL1, we performed multi-colour live super-resolution microscopy via Super Resolution by Radial Fluctuations (SRRF) [31] of APPL1 and EEA1 (Supplementary Movie 5). Interestingly, we observed that the APPL1 and EEA1 are counter-clustered (Figure 3b). Both APPL1 and EEA1 show dynamic localisation with time, but this counter-clustering is maintained through the process of conversion, until the APPL1 signal is lost (Figure 3b,c).

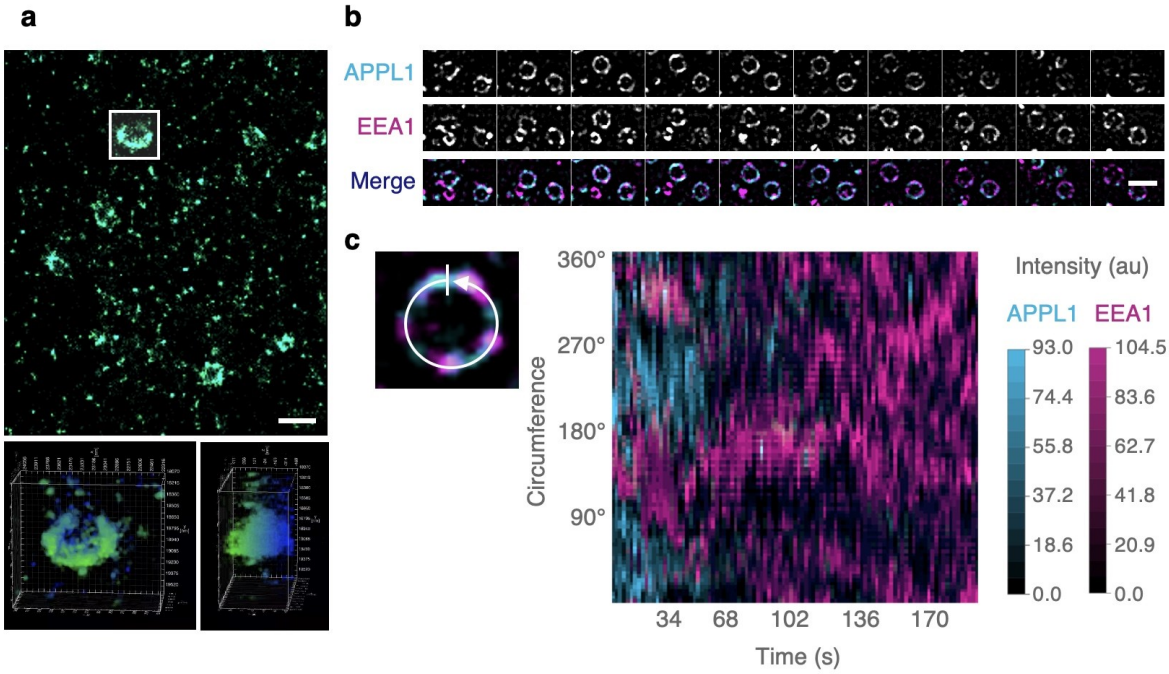

Figure 3. APPL1 and EEA1 exhibit dynamic counter-clustering when imaged using super-resolution microscopy. a) 3D PALM imaging of Dendra2-EEA1 shown as a maximum intensity projection (*top*) and as a 3D volume (*bottom*). Intensity is colour-coded to *z* position. Scale bar = 1 µm. **b)** Montage of live SRRF experiment showing dynamic APPL1 (*cyan*) and EEA1 (*magenta*) clustering. Scale bar = 1 µm. **c)** Kymograph of line intensity plot of normalised APPL1 (*cyan*) and EEA1 (*magenta*) intensity of a converting APPL1 endosome imaged with SRRF, after processing. Circumference position in degrees is plotted on the *y* axis, as indicated in the schematic (*left*), and time in seconds is plotted on the *x* axis.

Taken together, our experimental observations suggested that heterotypic interactions contribute to the initiation of conversion processes and that a local threshold concentration for the first binding of EEA1 via its N-terminus may exist, which when overcome, triggers the phosphoinositide conversion reactions. This would allow generation of PI(3)P from PI(3,4)P2, thus enabling EEA1 to bind via its C-terminus, leading to complete APPL1 to EEA1 conversion. We thus hypothesised that the inter-endosomal binding ability of the EEA1 homodimer and the presence of heterotypic collisions may work together to seed conversions. EEA1 projects out into the cytoplasm due to its ~200 nm long coiled-coil domain [19, 22]; furthermore, it can bind to endosomal membranes at both its N- and C-terminal ends [32]. Whilst at the C-terminal domain, EEA1 binds to membranes through the coincidence detection of Rab5 and PI(3)P [22, 33, 34], at the N-terminus, EEA1 solely binds to Rab5 through a zinc finger-binding domain [22, 35]. We therefore rationalised that in a heterotypic collision, the incident APPL1 endosome would have little to no PI(3)P and as such the only EEA1 binding that is probable is through N-terminal binding, thus producing an encoded precedence in EEA1 N- versus C-terminal binding.

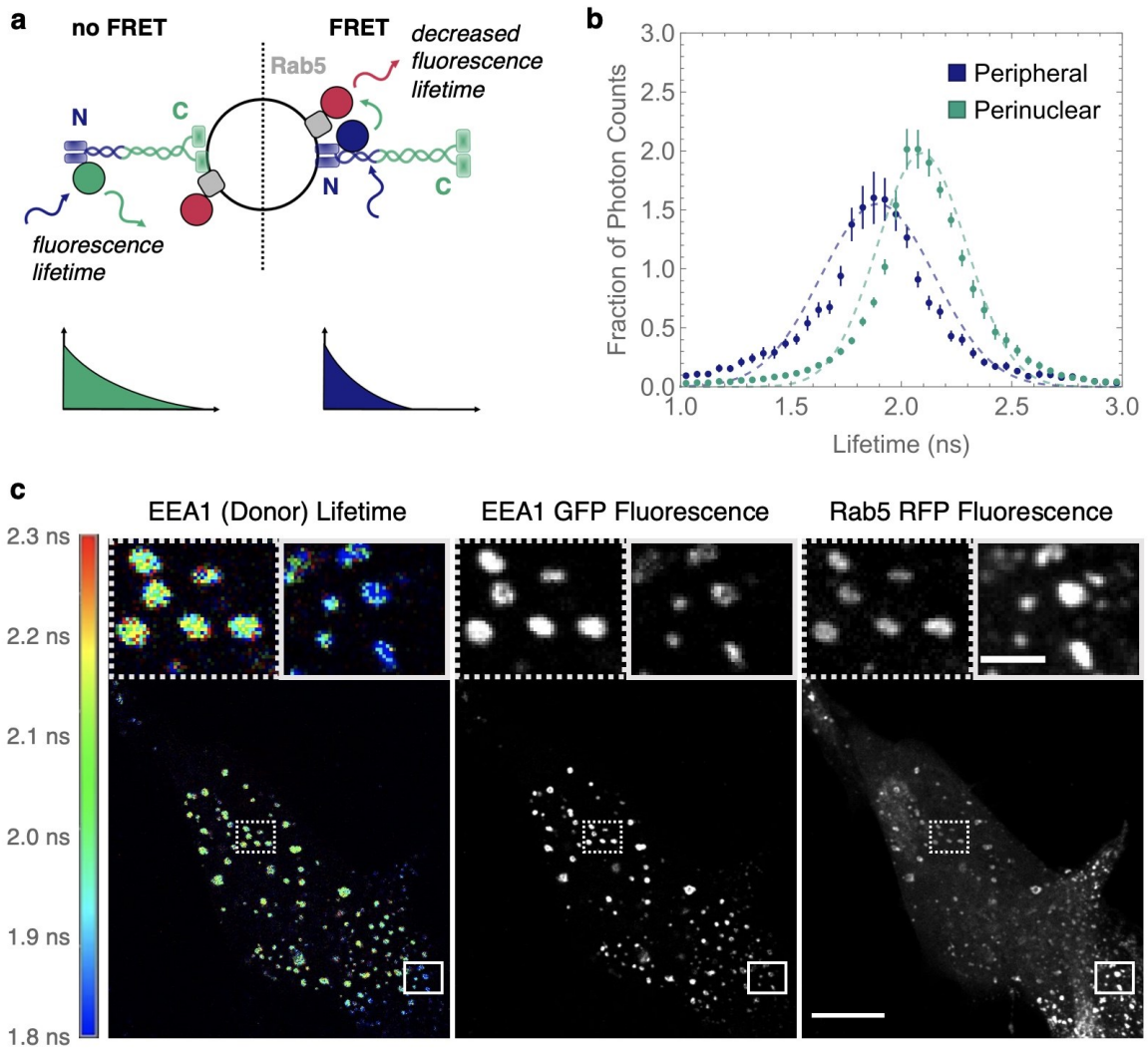

Figure 4. EEA1 endosomes exist in two spatially distinct populations characterised by opposite membrane binding. a) Schematic diagram of EEA1 FLIM experiment logic. Shorter fluorescence lifetime (*right*) indicates a FRET interaction between EEA1-EGFP and Rab5-RFP and therefore indicates EEA1 is bound via its N-terminal binding domain. Correspondingly, longer fluorescence lifetime (*left*) indicates no FRET interaction and thus that EEA1 is bound via its C-terminal binding domains to the membrane. **b)** Normalised frequency histograms of the detected fluorescence lifetimes of EEA1-EGFP photons measured in peripheral endosomes (*blue*) and perinuclear endosomes (*green*); bars represent standard errors of the mean; dashed curves show Gaussian fits for reference. Mean lifetimes calculated from these data are 1.87 ns and 2.10 ns for the peripheral and perinuclear curves, respectively. Endosomes were measured across n = 6 cells. **c)** Representative FLIM-FRET experiments of RPE1 cells transfected with EEA1-EGFP and Rab5-RFP. Coloured scale bar represents donor lifetime ranging from 1.8 ns (*blue*) to 2.3 ns (*red*). Left panel shows the FLIM image of EEA1 (donor) lifetime, middle panel shows EEA1 fluorescence intensity and right panel shows Rab5 fluorescence intensity; boxes indicate the regions of the zoomed insert. Scale bar = 10 µm. Zoomed insert scale bar = 1 µm.

To determine which terminus of EEA1 is bound to the already EEA1 positive endosome and which domain binds to the incoming nascent endosome, we utilised fluorescence lifetime microscopy (FLIM). We reasoned that N-terminally tagged EGFP-EEA1 combined with an RFP FRET partner, could distinguish N- from C-terminal binding using the lifetime of EGFP, since EEA1 is 200 nm long in its straight conformation and it binds directly to Rab5 via its N-

terminal (Figure 4a). Multi-scale molecular dynamics simulations also suggest that the coiled coil domain can extend with a tilt up to 50° from the normal to the endosomal membrane surface when bound using the C-terminal FYVE binding domain [36]. Thus, N-terminal binding will result in decreased fluorescence lifetime due to FRET with Rab5 labelled with RFP, whereas C-terminal binding will show the EGFP lifetime since no FRET will take place. We first investigated whether different populations of EEA1 positive endosomes, bound via N- or C- termini, exist in fixed cells. We found that EEA1 endosomes showed two strikingly distinct populations: C-terminally bound EEA1 that localised closer to the nucleus of the cell (Figure 4c), and N-terminally bound EEA1 that was predominantly peripherally localised (Figure 4b, c). Additionally, we were able to detect these same two populations of endosomes using the inverse FRET pair using Rab5 EGFP lifetime in cells transfected with EEA1-TagRFP, in contrast to cells transfected with only EEA1-EGFP (Supplementary Figure 4). These experiments strongly indicate that the newly generated endosomes have the first EEA1 binding via the N-terminus.

To map the temporal dynamics of EEA1 binding via the N- or C-terminals, we performed live-cell FLIM of EGFP-EEA1 and Rab5-mRFP. However, live-cell FLIM using confocal microscopy with sufficient temporal resolution to capture endosomal processes intrinsically results in a reduced number of collected photons. To overcome this, we took advantage of *a priori* knowledge from fixed cell experiments and fit live-FLIM data with the two lifetime components detected in fixed experiments. This gave a shorter lifetime component corresponding to N-terminally bound EEA1, where GFP can 'FRET' with Rab5-RFP, and a longer fluorescence lifetime corresponding to C-terminally bound EEA1, where the N-terminal is at least 150 nm away, extended into the cytoplasm from the Rab5 RFP. We then separated the detected photons collected at each pixel based on these two components, effectively giving an 'NT EEA1' and a 'CT EEA1' channel (Figure 5a). Using this fitting, we visualised the initial appearance of EEA1 on Rab5-positive, EEA1-negative endosomes following a collision-conversion event. We observed that only N-terminally bound EEA1 (Figure 5a, b, Supplementary Movie 6, 7) localised on these Rab5-positive endosomes and displayed an increasing signal of C-terminally bound EEA1, concomitant with fusions and trafficking towards the perinuclear region (PNR) (Figure 5d, e, Supplementary Movie 8). This gradual acquisition of C-terminal EEA1 seen through the increase in longer lifetime components and reduced N:C intensity ratio (Figure 5e) suggests a concurrent phosphoinositide conversion of PI(3,4)P2 into PI(3)P, with the initial trigger via N-terminally bound EEA1, even for unaided conversions.

Whilst EEA1-EEA1 fusions are commonly observed, by separating EEA1 vesicles into their constituent N- and C-terminally bound populations, we observed that fusions primarily occurred when at least one vesicle had C-terminal EEA1 present (Figure 5c). Fusions were most likely to occur between N- and C- terminal EEA1-positive or C- and C- terminal EEA1-positive endosomes (Figure 5c). Endosome pairs with at least one EEA1-negative endosome did not show significant fusions. Remarkably, in cases with both endosomes N-terminally positive, no significant fusions were observed. Two conclusions could be drawn from these results. First, the requirement of at least one C-terminally bound EEA1 and non-fusion of N-terminally bound EEA1-positive endosomes suggest that cross-binding of EEA1 is a necessary step for endosomal fusions to occur [19, 22]. This aligns with previously published results showing that both ends of the endosomal tether must be stably bound to result in endosomal fusion [19, 22]. Second, the appearance of N-terminally bound EEA1 prior to C-terminally bound EEA1 in cases of unaided conversions indicates that the N-terminal binding

is a necessary and intermediate step before further undergoing a maturation via phosphoinositide conversion into C-terminally bound EEA1.

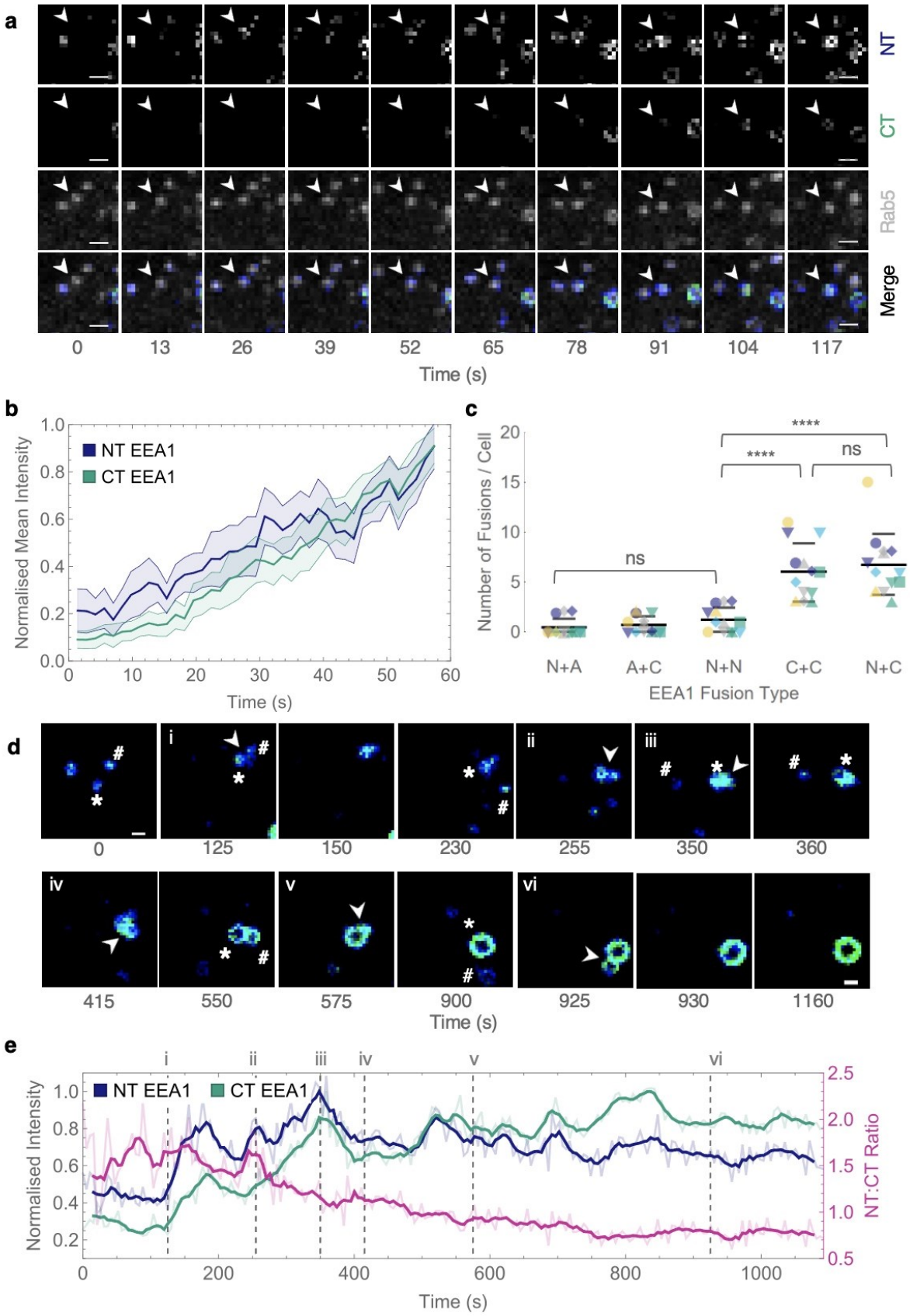

Figure 5. EEA1 initially binds via its N-terminal binding domain before maturing into a C-terminal bound endosome. a) Representative montage showing the appearance of N-terminal EEA1 following collision-conversion, imaged by live FLIM-FRET as described in Figure 4a. EEA1-EGFP fluorescence lifetime has been fit with a two-component regression (τ_1 = 1.006 ns, τ_2 = 2.600 ns). The image has been pseudo-coloured by the relative photon contribution from each component; the shorter N-terminal EEA1 component (*blue*), the longer C-terminal EEA1 component (*green*), and Rab5-RFP fluorescence (*grey*). Arrow indicates nascent converting endosome. Scale bar = 2.5 µm, time is measured in seconds. **b)** Normalised mean intensity plot of converting endosomes following seeding at time = 0. Line graphs show mean intensity of N-terminally bound EEA1 (*blue*) and C-terminally bound EEA1 (*green*), area fill indicates 95% confidence interval at each time-point. Time is measured in seconds. *n* = 20 conversion events. **c)** Fusions are categorised by the participating endosomes; N-terminal bound (N), C-terminal bound (C) and EEA1 absent, Rab5-positive (A). Plots show mean, error bars indicate S.D. Each coloured shape indicates a different cell, *n* = 13. ns indicates non-significant difference, **** indicates p<0.0001. Each mean was compared against the others using an ordinary one-way ANOVA. **d)** Representative montage of EEA1 N- to C-terminally bound conversion. N-terminally bound EEA1 (*blue*), C-terminally bound EEA1 (*green*). Arrows indicate points of fusion as numbered in panel e, asterisks indicate 'main' endosome corresponding to the intensity trace, hashes show incident endosomes prior to fusion. Scale bar = 2.5 µm, time is measured in seconds. **e)** Intensity trace of N- to C-terminally bound conversion corresponding to montage in panel d. Lines indicate mean relative lifetime amplitudes of N-terminal EEA1 (*blue*), C-terminal EEA1 (*green*) and the N:C intensity ratio (*magenta*), bold lines indicate 3-frame moving average; intensities were manually measured for each endosomal pixel. Dotted lines indicate successive fusion time-points. Time is measured in seconds.

To validate the consistent observation of N-terminal binding of EEA1 as a prior to any maturation process and to investigate the stringency in requirement of N-terminal binding of EEA1 via Rab5 in maturation, we used an N-terminal mutant of EEA1 carrying F41A and I42A at the C_2H_2 Zn^{2+} site (EEA1 Nt-mut), which is impaired in Rab5 binding [37]. When expressed in wild-type RPE1 cells, conversions were unimpaired and endosomal fusions were only mildly affected. This suggested that the Rab5 binding mutant, EEA1 Nt-mut, did not display a strong dominant negative phenotype and that the endogenous EEA1 could still function to evince endosomal maturations (Figure 6). This could be due to the fact that the observed clustering buffers against dysfunctional mutant EEA1; in addition, as EEA1 is a homodimer, it may still have one binding site active. Therefore, we utilised a HeLa EEA1 KO cell line and transiently expressed EEA1 Nt-mut. In contrast to wild-type EEA1, EEA1 Nt-mut exhibited no heterotypic interactions that resulted in maturations per cell over 20 minutes. Furthermore, no EEA1 signals were observed on APPL1 endosomal trajectories, suggesting that the collision-triggered conversion mechanism was dysfunctional owing to impaired Rab5 binding at the instance of collision. It is also to be noted that the expression of EEA1 Nt-mut resulted in larger but fewer and less motile endosomes (Supplementary Movie 8). If only the C-terminus of EEA1, via its Rab5 and FYVE binding, were involved in the phosphoinositide governed conversion, we would expect to detect some APPL1 to EEA1 conversions. In our experiments, unaided conversions were also completely abrogated, indicating that, even in direct conversions, where collisions may not play a role, the N-terminal binding is a compulsory intermediate step.

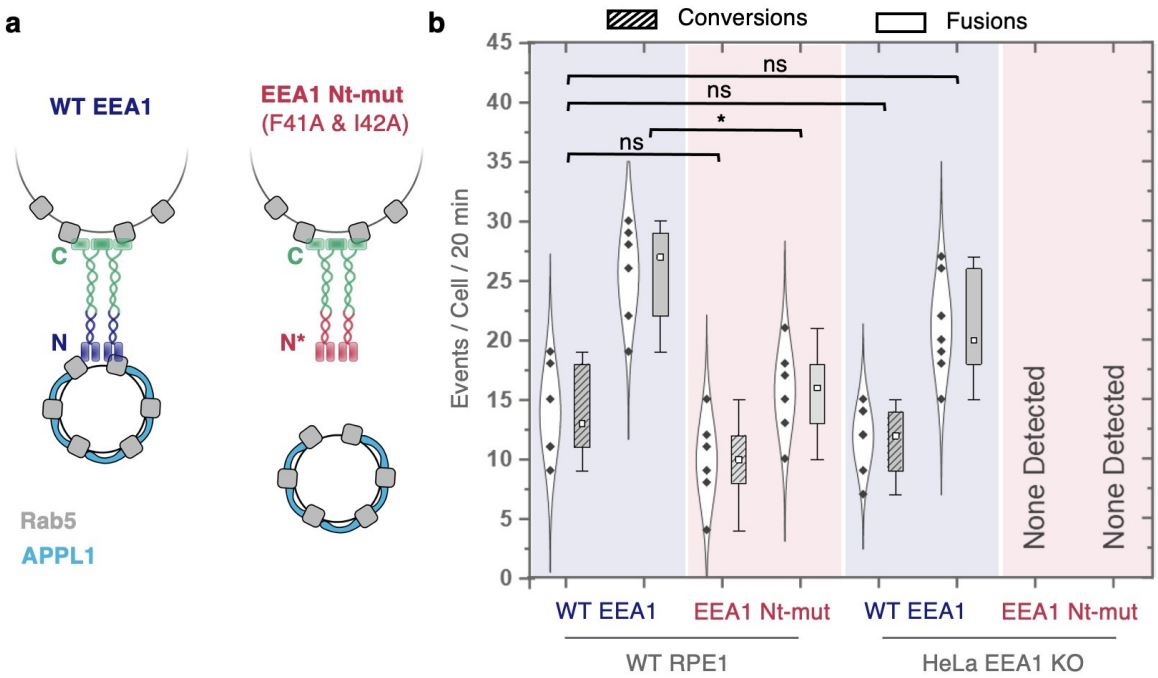

Figure 6. The initial N-terminal of EEA1is essential for endosomal conversions. RPE1 wild-type cells and HeLa EEA1 knockout (KO) cell lines expressing wild-type EEA1 (blue) or N-terminal mutant deficient in binding Rab5 (red) were imaged using LLSM and the total number of conversions and fusions were quantified. ns indicates non-significant difference, * indicates $p<0.05$. Each mean was compared against the others using an ordinary one-way ANOVA. In the case of HeLa EEA1 KO cells expressing EEA1 N-terminal Rab5 binding mutant, no events were detected by the analysis workflow or by visual inspection.

To summarise, collisions between endosomes form an important step in overall endosomal conversions rates. The live FLIM data suggests that N-terminally bound EEA1, via interaction with Rab5, is a step preceding the phosphoinositide-based binding of EEA1 via its C-terminal FYVE domain (Figure 5). Expressing the N-terminal Rab5 binding mutant in HeLa EEA1 KO did not rescue any maturation events, suggesting that this is a necessary step (Figure 6). Additionally, super-resolution imaging suggests clustered distribution of EEA1, as well as counter-clustering of APPL1 to EEA1 (Figure 3). This suggests the presence of feedback in the reaction scheme that governs progressively preferential EEA1 binding over APPL1binding. To construct a plausible model that agrees with our experimental observations as well as the known protein-protein and protein-membrane interactions of the components involved, we designed a computational model that captures the complex interplay between the distinct phosphoinositide molecules, Rab5, APPL1 and EEA1, and the phosphoinositide conversion (Figure 7). Importantly, we consider the N-terminal domain of EEA1, which was observed to bind first in unaided collisions as well as in aided conversions through collisions. To simulate this system, we used a grid on the surface of a sphere with two layers of nodes; a layer of Rab5 and a phosphoinositide layer which began as PI(3,4)P2 but could be converted to PI(3)P by INPP4A if unbound [9]. Binding to these layers of nodes were the agents, each with a different attachment and detachment rate depending on the nodes present; APPL1 (binding Rab5 and PI(3,4)P2), N-terminal EEA1 (binding Rab5) and C-terminal EEA1 (binding Rab5 and PI(3)P). The interaction map of agents and nodes is shown in Figure 7a. Using this reaction scheme, we were able to simulate the reactions and tune the parameters to

recapitulate the experimentally observed conversion dynamics as well as formulate the effects of the 'trigger and convert' mechanism (Supplementary Movie 9).

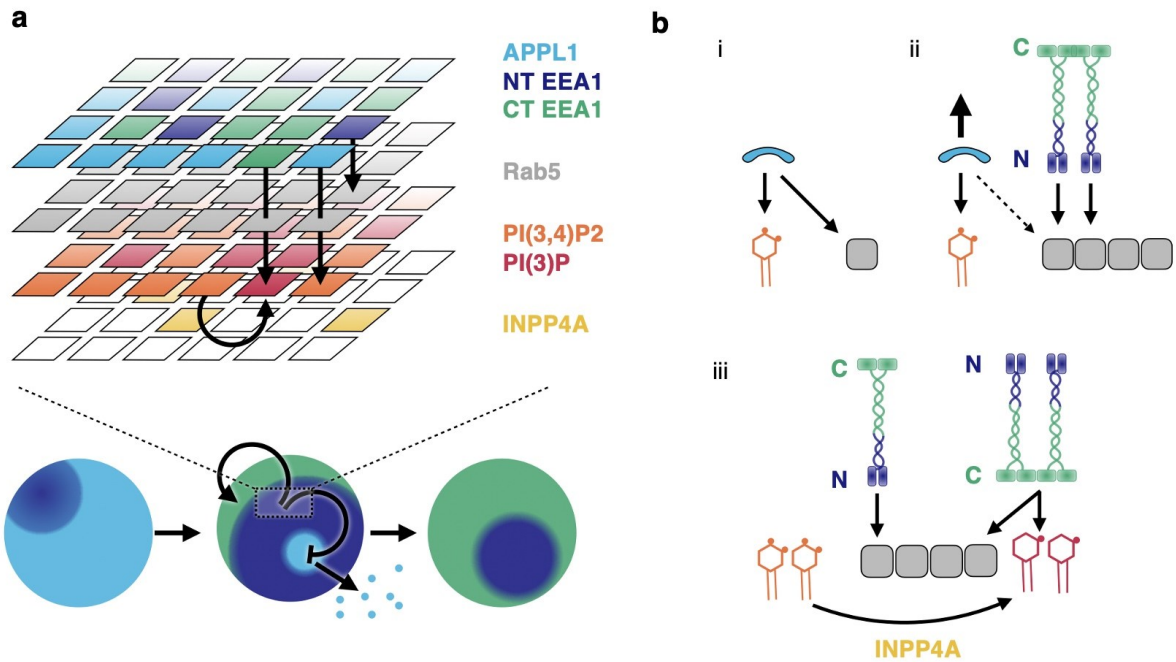

Figure 7. Interaction map of agents and nodes used in simulations. Schematic of agent and node logic used in modelling. **a)** The endosome is simulated as a multi-layered surface of a sphere, where different layers are occupied by different agents and nodes, as shown. The sphere is initially dominated by APPL1 attachments (*cyan*), which over time are replaced by N-terminal EEA1 (*dark blue*), and finally C-terminal EEA1 (*green*). **b)** APPL1 and EEA1 stochastically bind and unbind, competing for Rab5 (*grey*) binding availability. (i) APPL1 requires both Rab5 and an adjacent PI(3,4)P2 (*orange*) to attach. (ii) N-terminal EEA1 replaces APPL1 in binding to Rab5 and frees up PI(3,4)P2. (iii) INPP4A (*yellow*) converts free PI(3,4)P2 to PI(3)P (*red*). C-terminal EEA1 requires Rab5 and an adjacent PI(3)P to bind.

Figure 8 shows an example trajectory, beginning with a very early endosome that is APPL1-positive and bound to PI(3,4)P2 and Rab5 via its PH-BAR domain. Spontaneous binding of INPP4A to this endosome can result in conversion of PI(3,4)P2 to PI(3)P; however, with APPL1 occupying most PI(3,4)P2, most INPP4A remains unbound and, therefore, inactive on its substrate. APPL1 can be transiently displaced by N-terminal EEA1, which binds directly to Rab5. Due to the inclusion of a positive feedback switch to mimic the experimentally observed clustering, APPL1 endosomes are relatively stable (Figure 8a). However, upon the introduction of a large pool of EEA1 as the result of a collision (Figure 8b), N-terminal EEA1 can sequester Rab5, thus destabilising the APPL1-Rab5 interactions and resulting in APPL1 desorption (Figure 8c). Consequently, INPP4A can now bind to its substrate PI(3,4)P2 and convert it into PI(3)P (Figure 8d). This leads to the binding of EEA1 through its C-terminal FYVE binding domain, as well as Rab5 binding (Figure 8e, f). In this scheme, the N-terminal binding of EEA1 acts as a trigger. Moreover, since the N-terminus of EEA1 has weak binding affinity to Rab5, we reasoned that the clustered organisation of EEA1 on endosomes, and the interaction of multiple N-terminal EEA1 at the instance of collision results in overwhelming the APPL1-Rab5 on the incoming endosome. We simulated the net decrease in conversion time of a single endosome that underwent one collision (Figure 9a), and the net decrease in

conversion time of endosomes in a cell allowed to collide randomly at increasing collision frequencies (Figure 9b).

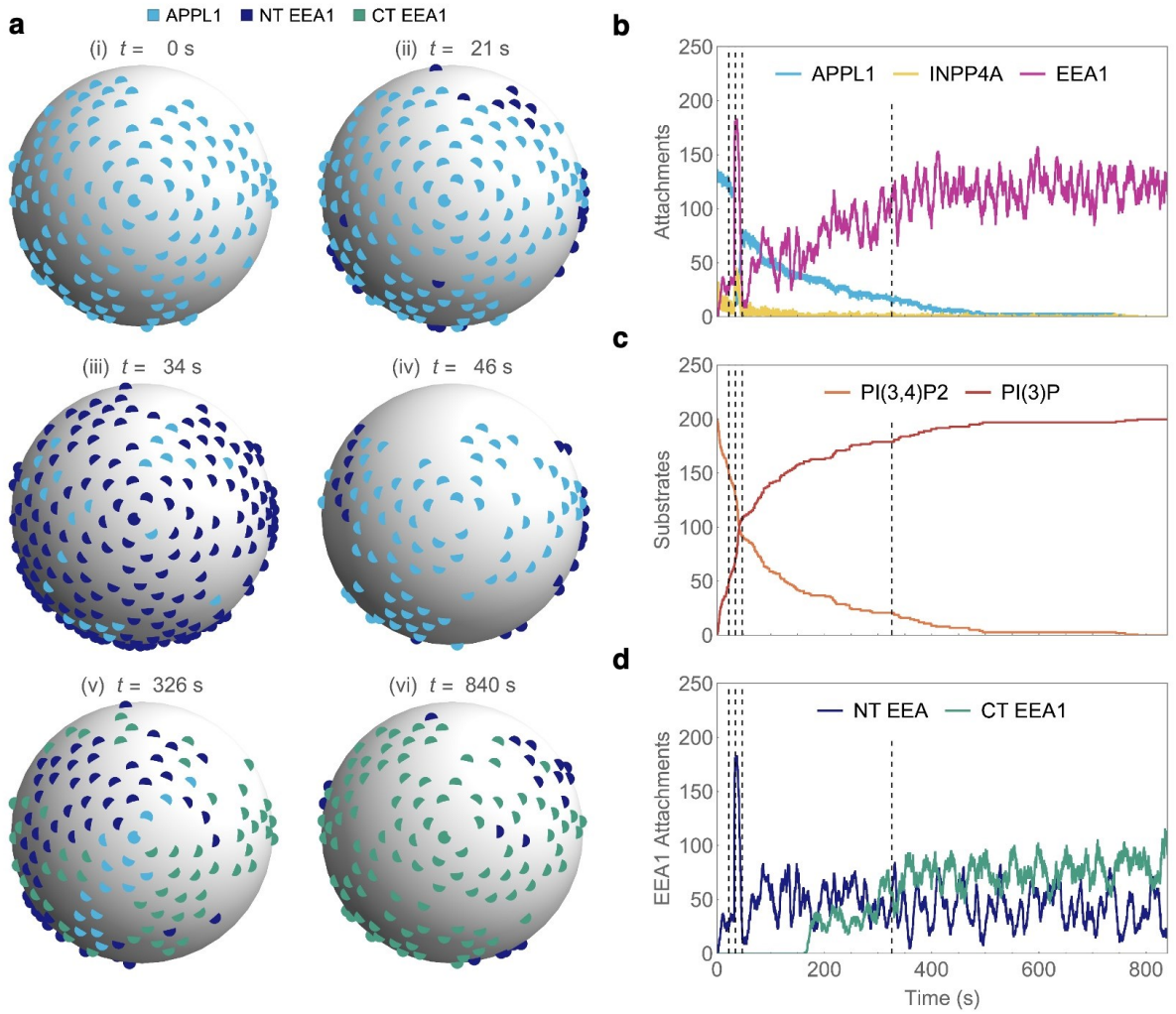

Figure 8. An example maturation time course of a simulated endosome undergoing collision. a) Surface of the simulated endosome at different time-points (marked by dashed lines in panels b–d), showing the attached APPL1 (*cyan*), N-terminal EEA1 (*dark blue*), and C-terminal EEA1 (*green*). Initially, the endosome is dominated by APPL1 (i), while N-terminal EEA1 attach in clusters (ii). Upon collision (which takes place at 31.5 s in this instance), there is a large influx of EEA1 N-terminal attachments (iii), which shortly detach due to cluster detachment (iv). However, this duration is sufficient to displace a large number of APPL1, allowing INPP4A to accelerate conversion of PI(3,4)P2 to PI(3)P. Eventually, C-terminal EEA1 attach in clusters (v) and ultimately dominate over N-terminal attachments (vi). **b)** Time series of numbers of attached APPL1, INPP4A and total EEA1 (including both N- and C-terminal attachments). **c)** Time series of numbers of PI(3,4)P2 and PI(3)P molecules on the endosome's surface. PI(3)P molecules are formed by a 1:1 conversion from PI(3,4)P2 by INPP4A. **d)** Time series of numbers of N- and C-terminal attachments of EEA1. Initially, most attachments are through N-terminal EEA1, while over the course of endosomal conversion, C-terminal attachments eventually become a majority. Collision mainly introduces new N-terminal attachments. For a dynamic version of this figure, refer to Supplementary Movie 9.

These simulations showed that clustering has a two-pronged effect on accelerating conversion. If a Rab5 molecule originally surrounded by bound APPL1 is occupied by EEA1, it will become unavailable for binding to APPL1. This creates a 'hole' in the APPL1 layer, which

decreases the binding affinity of APPL1 in the region surrounding the hole (as compared to a region filled by APPL1, since clustering increases the binding affinity of a species in accordance with the local density of that species). This in turn increases the chance that the hole will expand. On the other hand, clustering of EEA1 attracts more EEA1 to the vicinity of the 'hole'. These two factors speed up the local back-and-forth conversion between APPL1 and EEA1 clusters, which increases the windows of opportunity for INPP4A to convert PI(3,4)P2 to PI(3)P. A heterotypic fusion between endosomes with N-terminally bound EEA1 and C-terminally bound EEA1, as observed in the live FLIM experiments (Figure 5c,d) represents only a state with higher N- to C- EEA1 ratio and the reaction scheme will proceed to convert the transiently increased PI(3,4)P2 to PI3P, subsequently replacing N-terminally bound EEA1 by C-terminally bound EEA1. Through our simulations, we were able to quantify the net decrease in conversion time due to clustering (Figure 9a). Once a sufficient number of PI(3,4)P2 have converted to PI(3)P, C-terminal attachments dominate since they have a stronger binding affinity, and they require both PI(3)P and Rab5 to bind, rendering Rab5 unavailable for N-terminal attachments.

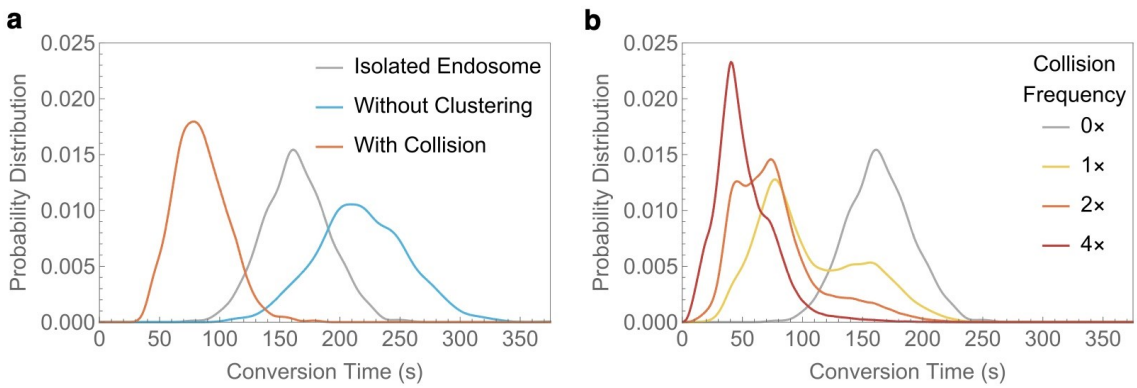

Figure 9. Investigating the effect of clustering and collision on the conversion time of endosomes through simulations. a) Conversion time distributions of simulated isolated endosomes. If the clustering mechanism of EEA1 molecules is removed from the simulation, the conversion time distribution shifts to the right (from grey to cyan), indicating slower conversions. If the isolated endosome is made to undergo collision (which takes place at t = 31.5 s for these simulations), the conversion time distribution shifts to the left (from grey to orange) and conversion time is reduced by almost one third. **b)** Conversion time distributions of a simulated cell in which endosomes collide randomly at a given collision frequency. The grey curve shows the case for no collisions. Upon increasing the collision frequency, the weight of the conversion time distribution shifts further to the left (towards red). There are multiple modes in the conversion time distribution corresponding to the number of collisions the endosome experienced before conversion. The leftmost mode lying between 20–50 s corresponds to two collisions before conversion, the middle mode lying between 60–100 s to a single collision, and the rightmost mode lying between 130–200 s to zero collisions.

DISCUSSION

The endosomal system is highly dynamic, requiring successive biochemical maturations of key lipids and associated proteins to achieve correct targeting of internalised cargo. Whilst the order of appearance of key species has been diligently identified for early endosomes, how the timing of maturation is maintained for each generated vesicle had not been studied. In this work we describe a novel mechanism that ensures timely maturation of vesicles at a whole

cell level. Specifically, we present a new trigger-and-convert model of APPL1 to EEA1 early endosomal maturation, as summarised in Figure 10.

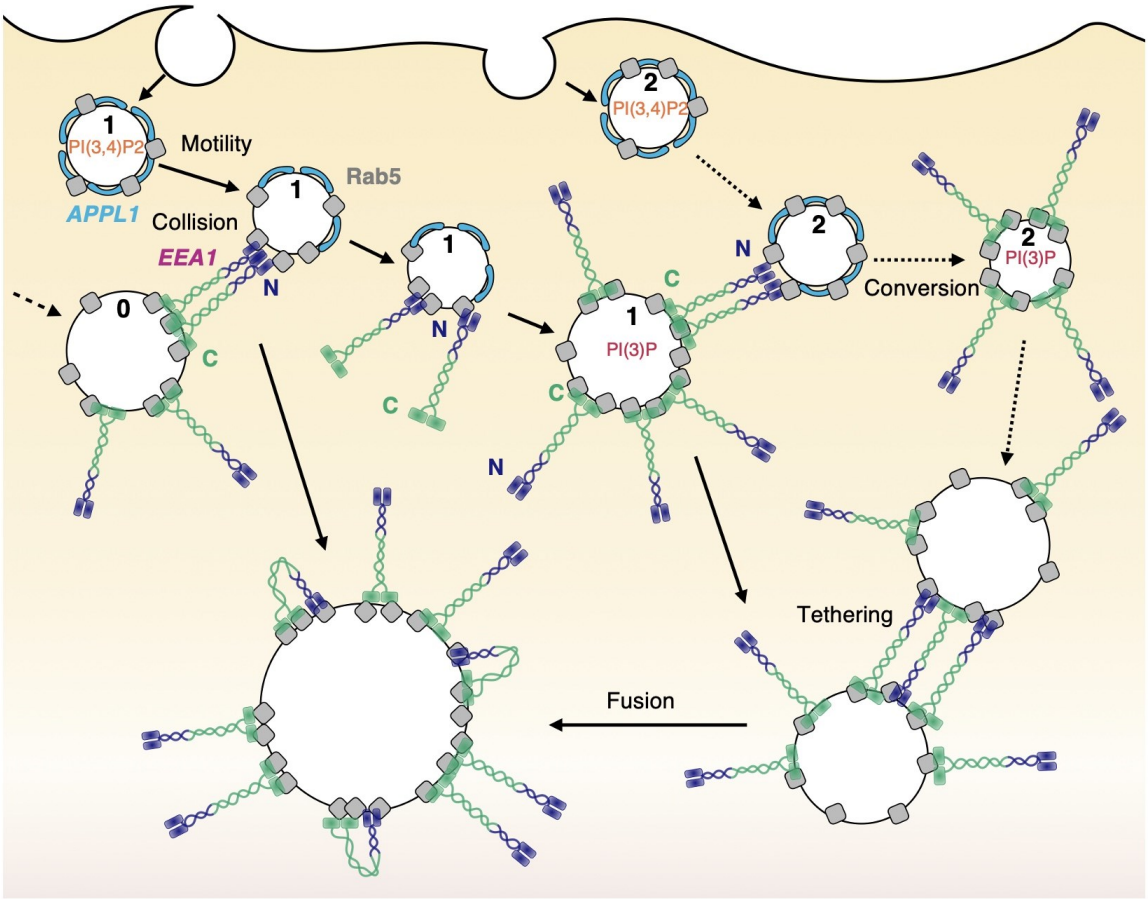

Figure 10. Summary of proposed EEA1 'trigger-and-convert' mechanism of maturation. Very early endosomes formed at the cell periphery (endosome 1) have PI(3,4)P2 (*orange*) containing membranes and APPL1 (*cyan*) bound to Rab5 (*grey*). These vesicles collide with mature EEA1 vesicles (endosome 0), seeding N-terminally bound EEA1 and triggering the conversion process. This enables the production of PI(3)P (*red*) and the binding of C-terminal EEA1. These vesicles can trigger conversions on nascent APPL1 vesicles (endosome 2) and participate in canonical endosomal tethering and fusion processes (bottom endosomes).

In this model, nascent APPL1 positive PI(3,4)P2 very early endosomes (VEEs) undergo active transport along microtubules and collide stochastically with mature EEA1 early endosomes (EEs). This collision is a 'trigger' that primes the VEE for maturation. Our experimental observations are consistent with a model whereby following such a collision, a cluster of EEA1 is transferred onto the incident VEE. This model is in conjunction with the following molecular details of EEA1. First, C-terminal EEA1 has a rigid quaternary structure that ensures that the coiled coil region extends into the cytoplasm, preventing the N-terminus from folding back and binding to Rab5 on the same endosome [19]. This would result in the N-terminus of EEA1 being located at 160–180 nm from the endosome surface [22], in agreement with observations of two distinct EEA1 populations made in our FLIM experiments. Second, EEA1 possesses two distinct Rab5 binding sites—one corresponding to the $C_2H_2\,Zn^{2+}$ finger at the N-terminus and the other overlapping with the PI3P binding FYVE domain at the C-terminus. The C-

terminal end also contains a calmodulin (CaM) binding motif. The N-terminus forms the stronger Rab5 interaction, while the C-terminus interaction, owing to the FYVE domain, operates on a coincidence detection mechanism resulting in specificity to PI3P-containing vesicles. While the exact steps at the instant of collision is beyond the scope of this manuscript, it is conceivable that a collision would result in the stronger N-terminus–Rab5 interaction overriding the C-terminus interactions. Furthermore, an unexplored but plausible mechanistic detail lies in the interactions of Ca^{2+}/CaM with Rab5 and the C-terminus of EEA1, which antagonises PI3P binding, and may operate to release C-terminus binding when the N-terminal interactions take place as a result of collision [38, 39]. Whether transient Ca^{2+} spikes operate to mediate transfer of molecules remains an attractive detail to investigate.

Post collision, the sequestration of Rab5 via N-terminal EEA1 results in desorption of APPL1 clusters. The reduced APPL1 binding to Rab5 also exposes PI(3,4)P2 to be dephosphorylated by 4-phosphatases, producing PI(3)P. The most likely candidate for this reaction is INPP4A, since it has been localised to Rab5 positive EEs [5, 40]. This availability of PI(3)P now enables EEA1 to bind via its C-terminal FYVE domains, thereby resulting in the irreversible maturation to an EEA1 positive EE. This mature endosome is in turn able to trigger more conversions of APPL1 VEEs following collisions, thus ensuring continual maturation of this dynamic population of vesicles.

Consistent with other studies of descriptions of specific domains on endosomes, we observed that both VEE and EEs showed a counter-clustered APPL1 and EEA1 distribution. The hypothesis that clustering forms an important aspect in providing a more robust process was recapitulated through our simulations, and suggested to be essential for the timely conversion of these vesicles. An attractive hypothesis is that phosphoinositide clustering underlies the observed protein distributions, as phosphoinositide clustering has been demonstrated in other vesicular and tubular membrane entities [29]. Additionally, Rab5 has also been suggested to be clustered [28]. A clustered distribution of EEA1 or its binding partner in the incident endosome, Rab5, would ensure that following a collision, a higher probability of transfer of EEA1 molecules exists. Furthermore, this would produce large fluctuations of EEA1 intensity on a converting endosome, as observed in our imaging movies.

Previous studies have shown that stochastic fluctuations have a significant effect on trafficking and maturation processes [14]. The greater the stochasticity in a system, the more the system dynamics favour non-steady state biochemical maturation over steady state vesicular exchange in cellular transport pathways. Biochemical maturation is characterised by a first passage time event in which the first instance of complete maturation of the compartment in question marks a point of no return. But the noise due to the inherent stochasticity in the system poses challenges to robust directional flow of material, which requires tight regulation on exchange processes between organelles. It was shown by Vagne and Sens that the presence of positive feedback in the maturation process can significantly suppress the stochastic fluctuations, and Golgi cisternae used homotypic fusions as the likely mechanism to overcome this challenge [14]. In a similar vein, our proposed mechanisms of clustering, collision, and heterotypic fusion, each provide positive feedback to the maturation process and are essential in the robust functioning of the exchange processes through noise suppression.

A relevant protein complex to this work is the mammalian class C core vacuole/endosome tethering (CORVET) system, which functions to mediate endosomal fusion independently of

EEA1 [41]. Surprisingly, overexpression of the N-terminal mutant of EEA1 also resulted in a similar phenotype of smaller, more fragmented APPL1 endosomes, with the exception that we found no APPL1-EEA1 double positive endosomes. It is unclear at what stage CORVET operates, and dissection of this question is beyond the scope of this study. However, the strong phenotype observed for the N-terminal mutant of EEA1 reinforces the role of EEA1 in self-regulating APPL1 to EEA1 conversion.

What is the physiological relevance of this mechanism? The trigger-and-convert approach provides emergent regulation of the timing of early endosome maturation, leading to a tightly controlled and a more timely and consistent flux of maturation, able to overcome the intrinsic stochasticity of single molecule protein–protein and protein–membrane interactions. This is critical as early endosomes act as stable sorting centres of endocytosed material, from which cargo is redirected towards the plasma membrane or sent towards late endosomes and lysosomal degradation. As a result, robust maturation of cargo-bearing vesicles is a requirement of the intracellular transport system. Furthermore, it has become increasingly apparent that many diverse transmembrane receptors are able to signal from within endosomes [42-47] and that signal attenuation may rely on the trafficking to distinct intracellular destinations or organelles [48, 49]. This suggests that the trafficking and maturation rate of endosomes is intrinsically coupled to the downstream signal transduction of transmembrane receptors [49-51], further highlighting the importance of tightly regulated intracellular transport itineraries that include transport and maturation [52, 53].

Our work highlights the power of rapid-volumetric imaging, coupled with an unbiased analysis pipeline and complemented by simulations, to capture and describe dynamical processes and thus unravel mechanisms in unperturbed systems, without the need for genetic and pharmacological alterations that lead to the establishment of a new steady state or phenotype, and thus may obscure the very dynamics that are to be studied. Emergent phenomena are central to biological processes across scales, and there is increasing evidence for structure-function relationships that extend far beyond molecular scales to form larger-scale patterns in space and/or time. In the endosomal system, the biochemical process of conversion is underpinned by phosphoinositide chemistry at the individual endosome level; at a population level, however, it is governed by the physical process of stochastic collisions that forms an inherent part of the transport system of endosomes. Furthermore, it suggests that the robustness of the intracellular transport network may not be derived solely from so-called ‘master regulators’ but through the complex dynamic interactions of individually noisy components to create emergent reproducibility of large-scale processes.

METHODS

Cell lines

RPE1 and HeLa EEA1 knockout (KO) cells were incubated at 37 °C in 5% CO_2 in high glucose Dulbecco’s modified Eagle’s medium (DMEM) (Life Technologies), supplemented with 10% foetal bovine serum (FBS) and 1% penicillin and streptomycin (Life Technologies). Cells were seeded at a density of 200,000 per well in a six-well plate containing 25 mm or 5 mm glass coverslips.

Live cell imaging

Cells were imaged using a lattice light sheet microscope (3i, Denver, CO, USA). Excitation was achieved using 488-nm and 560-nm diode lasers (MPB Communications) at 1–5% AOTF transmittance through an excitation objective (Special Optics 28.6× 0.7 NA 3.74-mm immersion lens) and is detected via a Nikon CFI Apo LWD 25× 1.1 NA water immersion lens with a 2.5× tube lens. Live cells were imaged in 8 mL of 37 °C-heated DMEM and were acquired with 2× Hamamatsu Orca Flash 4.0 V2 sCMOS cameras.

Plasmids and transfection

Cells were transfected with pEGFPC1-human APPL1, a gift from Pietro De Camilli (Addgene plasmid #22198) [3]; EEA1 TagRFP-T, a gift from Silvia Corvera (Addgene plasmid #42635) [17]; EGFP-EEA1, a gift from Silvia Corvera (Addgene plasmid #42307) [33]; EGFP-Rab5, a gift from Marci Scidmore (Addgene plasmid #49888); and mRFP-Rab5, a gift from Ari Helenius (Addgene plasmid #14437) [54]. Cells were transfected with a total of 1 µg DNA (0.3 µg + 0.3 µg plasmid of interest + 0.4 µg blank DNA) using lipofectamine 3000 (Thermo Fisher Scientific). The DNA sequence for the N-terminal mutant of EEA1 carrying F41A and I42A, deficient in Rab5 binding was synthesised and cloned into the TagRFP-T vector using the XhoI/ BamHI sites. It has been reported that drastic over-expression of APPL1 or EEA1 results in colocalisation of APPL1 and EEA1 on Rab5 endosomes, we optimised this concentration by screening for this artefact, where we see no overlap of APPL1 and EEA1.

Fluorescence lifetime imaging

RPE1 cells were transfected with either EGFP-EEA1 + mRFP-Rab5 or EEA1 TagRFP-T + EGFP-Rab5; and either fixed with 4% paraformaldehyde or imaged live. The cells were imaged using an SP8 Falcon (Leica Microsystems) with an 86× 1.2 NA objective. Fluorescence lifetime images were acquired upon sequential excitation at 488 nm and 560 nm light using a tuneable pulsed white-light laser at 10% transmission, with emission collected at 500–550 nm and 580–630 nm, respectively, using two Leica HyD detectors. The GFP lifetimes were fitted using two-component fitting with τ_1 = 1.006 ns and τ_2 = 2.600 ns. The fixed images were analysed with pixel-wise lifetime fitting, and the live movies were analysed by separating the images into the two contributing fluorescence lifetime images.

Drug addition

Cells were incubated with 100 nM nocodazole in 8 mL Dulbecco's Modified Eagle Medium (DMEM) for 5 min before and during imaging as indicated. Cells were similarly treated with 100 nM phorbol 12-myristate 13-acetate (PMA) 5 min before and during imaging as indicated.

Super resolution by radial fluctuations (SRRF)

RPE1 cells transfected with APPL1-EGFP and EEA-T-TagRFP were stimulated with 100 nM PMA as detailed above. The cells were then imaged using widefield fluorescence microscopy with a Nikon Ti-2E body, 100× 1.5 NA objective (Olympus) and Prime 95B camera

(photometrics). Images were captured in 100 frame bursts with 5 ms exposure for each channel sequentially every 2 seconds for ~1 minute image periods. The images were then processed using the SRRF plugin for Fiji [31, 55].

Segmentation and tracking analysis

Datasets analysed consisted of LLSM six movies of untreated and two movies of nocodazole-treated RPE1 cells. Images were first deskewed, then adaptive histogram equalisation and a median filter applied prior to blob detection using the Laplacian of Gaussian operator. The expected range of object sizes were supplied as an independent parameter for each fluorescence channel, with other parameters tuned to return a preliminary set of over-detected blobs, defined by centres of mass and approximate radii. From these data, representative regions denoting endosomes and background, respectively, were chosen from each movie in an unsupervised manner (by choosing the brightest and dimmest blobs, respectively); these regions were then used as templates to calculate cross-correlations against each candidate endosome. The results of this operation define a set of features for each object, which were used as inputs to a *k*-means clustering algorithm to classify objects into endosomes versus background (Supplementary Figure 1).

A custom tracking routine built on trackpy and using both localisation and intensity information was then used to link objects into complete trajectories, independently for each channel. Events of interest were then calculated by trajectory analysis. Correlated trajectories were classified as potential conversions [52, 53], with stringent filters applied to exclude any events not clearly representative of APPL1–EEA1 conversions (Supplementary Figure 2a). To identify heterotypic collisions, local trajectories of neighbouring APPL1–EEA1 pairs were used to calculate the pairwise inter-endosome distance (separation between surfaces of nearby APPL1 and EEA1 endosomes along the line connecting their centres of mass). Local minima in the inter-endosome distance below a threshold value (within 200 nm, or roughly two pixels of overlap in the lateral dimension) were classified as collisions. These values were subsequently filtered to ensure that conversion-like events were excluded from the set of heterotypic collisions (Supplementary Figure 2b). Events showing APPL1–EEA1 conversions were classified as fusions or conversions based on whether the particular EEA1 track existed prior to colocalisation with APPL1, respectively. Events were classified as collision-induced versus unaided based on whether the APPL1 endosome collided with any EEA1 endosome in the 30 s prior to the event (Supplementary Figure 2c).

Photo-Activated Localization Microscopy (PALM)

Dendra-2 EEA1 was generated by replacing TagRFP-T in RagRFP-T EEA1 (Addgene plasmid #42635) at cloning sites AgeI and XhoI. Cells transfected with Dendra-2 EEA1 were fixed using 0.2% glutaraldehyde and 4% PFA in cytoskeletal buffer (10 mM MES, 150 mM NaCl, 5 mM EDTA, 5 mM glucose and 5 mM $MgCl_2$) for 15 minutes at room temperature. The cells were washed gently three times with PBS. PALM microscopy was carried out with a Nikon N-STORM microscope with a 100× oil immersion objective (1.49 NA) with a cylindrical lens for 3D localization. A 488 nm laser beam was used for pre-converted Dendra-2 excitation, with 405 nm for photoconversion and a 561 nm beam for post-photo converted Dendra-2. Localizations were exported to ViSP for visual examination and generating depth colour-coded images [56].

Simulations

The endosome's surface was simulated as a bi-layered Fibonacci Sphere (a spherical grid in which neighbouring points are approximately equidistant). One layer consisted of Rab5 and the other PI(3,4)P2 or PI(3)P. The agents (APPL1, INPP4A, and N- and C-terminally attached EEA1) were allowed to stochastically attach and detach according to the schematic shown in Figure 7. The attachment rates increased with the number of neighbouring agents of the same type (cluster attach), and detachment rates increased with the number of neighbouring agents of the same type that detached recently (cluster detach). In addition, INPP4A had a fixed probability of converting PI(3,4)P2 to PI(3)P, and a fixed probability of jumping to another nearby free PI(3,4)P2 after conversion. Upon collision, a fixed number of EEA1 N-terminal attachments were added to the endosome according to the availability of free Rab5 in a short time window after the collision. The conversion time of the endosome was measured as the first passage time of the fraction of PI(3,4)P2 converted to PI(3)P crossing a fixed threshold (set at 60%). See Supplementary Material for details.

ACKNOWLEDGEMENTS

The experimental work presented here was partially supported by the National Health and Medical Research Council of Australia (APP1182212) and ARC LIEF (LE150100163). H.M.Y. is supported by an Australian Government Research Training (RTP) Scholarship. A.P. and U.K.M. are supported by Monash Biomedicine Discovery Institute Scholarships. The EMBL Australia Partnership Laboratory (EMBL Australia) is supported by the National Collaborative Research Infrastructure Strategy of the Australian Government. The authors gratefully acknowledge the Imaging, FACS and Analysis Core and Cameron Nowell at Monash Institute of Pharmaceutical Science for their instrumentation and technical support. S.I.-.B., K.J. and C.S.W. thank the Purdue Research Foundation, Purdue University start-up funds, and the Ross-Lynn Fellowship award for financial support. S.A thanks Marino Zerial for the kind gift of HeLa EEA1 KO cell line and Samuel Rodgers for discussions. S.A. and S.I.-B. Thank all members of the Arumugam and Iyer-Biswas groups who contributed to discussions and gave feedback on the manuscript.

AUTHOR CONTRIBUTIONS

S.A. conceived of and designed the experiments, and oversaw all aspects of the project; S.I.-B. directed the theory efforts, simulations, and the development of the automated analysis pipeline; H.M.Y, U.K.M, and S.A. performed LLSM experiments, H.M.Y. performed fluorescence lifetime experiments, and H.M.Y. and S.A. performed super-resolution experiments; H.M.Y, K.J., C.S.W, H.G, A.P, and S.A. analysed the data; K.J. performed agent-based simulations to propose, verify, and fine-tune mechanism under the guidance of S.I.-B; C.S.W. developed the automated detection, tracking and analysis pipeline and workflow under the guidance of S.I.-B.; S.A. H.M.Y, U.K.M. and H.G. contributed to molecular biology; and H.M.Y, K.J., C.S.W., S.I.-B. and S.A. discussed results, helped shape the research and analysis, and wrote the manuscript.

REFERENCES

1. Huotari, J. and A. Helenius, *Endosome maturation.* The EMBO journal, 2011. **30**(17): p. 3481-3500.
2. Rink, J., et al., *Rab conversion as a mechanism of progression from early to late endosomes.* Cell, 2005. **122**(5): p. 735-49.
3. Zoncu, R., et al., *A phosphoinositide switch controls the maturation and signaling properties of APPL endosomes.* Cell, 2009. **136**(6): p. 1110-21.
4. Wallroth, A. and V. Haucke, *Phosphoinositide conversion in endocytosis and the endolysosomal system.* J Biol Chem, 2018. **293**(5): p. 1526-1535.
5. Shin, H.-W., et al., *An enzymatic cascade of Rab5 effectors regulates phosphoinositide turnover in the endocytic pathway.* The Journal of cell biology, 2005. **170**(4): p. 607-618.
6. Norris, F.A., R.C. Atkins, and P.W. Majerus, *The cDNA cloning and characterization of inositol polyphosphate 4-phosphatase type II. Evidence for conserved alternative splicing in the 4-phosphatase family.* J Biol Chem, 1997. **272**(38): p. 23859-64.
7. Norris, F.A., V. Auethavekiat, and P.W. Majerus, *The isolation and characterization of cDNA encoding human and rat brain inositol polyphosphate 4-phosphatase.* J Biol Chem, 1995. **270**(27): p. 16128-33.
8. Shin , H.-W., et al., *An enzymatic cascade of Rab5 effectors regulates phosphoinositide turnover in the endocytic pathway.* Journal of Cell Biology, 2005. **170**(4): p. 607-618.
9. Wang, H., et al., *Phosphatidylinositol 3,4-bisphosphate synthesis and turnover are spatially segregated in the endocytic pathway.* Journal of Biological Chemistry, 2020. **295**(4): p. 1091-1104.
10. Bright, N.A., M.J. Gratian, and J.P. Luzio, *Endocytic Delivery to Lysosomes Mediated by Concurrent Fusion and Kissing Events in Living Cells.* Current Biology, 2005. **15**(4): p. 360-365.
11. Duclos, S., et al., *Rab5 regulates the kiss and run fusion between phagosomes and endosomes and the acquisition of phagosome leishmanicidal properties in RAW 264.7 macrophages.* Journal of Cell Science, 2000. **113**(19): p. 3531-3541.
12. Redner, S., *A Guide to First-Passage Processes*. 2001, Cambridge: Cambridge University Press.
13. Iyer-Biswas, S. and A. Zilman, *First-Passage Processes in Cellular Biology*, in *Advances in Chemical Physics*. 2016. p. 261-306.
14. Vagne, Q. and P. Sens, *Stochastic Model of Maturation and Vesicular Exchange in Cellular Organelles.* Biophys J, 2018. **114**(4): p. 947-957.
15. Chen, B.-C., et al., *Lattice light-sheet microscopy: Imaging molecules to embryos at high spatiotemporal resolution.* Science, 2014. **346**(6208): p. 1257998.
16. Erdmann, K.S., et al., *A Role of the Lowe Syndrome Protein OCRL in Early Steps of the Endocytic Pathway.* Developmental Cell, 2007. **13**(3): p. 377-390.
17. Navaroli Deanna, M., et al., *Rabenosyn-5 defines the fate of the transferrin receptor following clathrin-mediated endocytosis.* Proceedings of the National Academy of Sciences, 2012. **109**(8): p. E471-E480.
18. Allan, D.B., et al., *soft-matter/trackpy: Trackpy v0.5.0.* Zenodo, 2021. **April**.
19. Murray, D.H., et al., *An endosomal tether undergoes an entropic collapse to bring vesicles together.* Nature, 2016. **537**(7618): p. 107-111.
20. Kalaidzidis, I., et al., *APPL endosomes are not obligatory endocytic intermediates but act as stable cargo-sorting compartments.* J Cell Biol, 2015. **211**(1): p. 123-44.
21. Mills, I.G., A.T. Jones, and M.J. Clague, *Involvement of the endosomal autoantigen EEA1 in homotypic fusion of early endosomes.* Curr Biol, 1998. **8**(15): p. 881-4.
22. Dumas, J.J., et al., *Multivalent endosome targeting by homodimeric EEA1.* Mol Cell, 2001. **8**(5): p. 947-58.
23. Callaghan, J., et al., *The endosome fusion regulator early-endosomal autoantigen 1 (EEA1) is a dimer.* The Biochemical journal, 1999. **338 (Pt 2)**(Pt 2): p. 539-543.

24. Zajac, A.L., et al., *Local cytoskeletal and organelle interactions impact molecular-motor- driven early endosomal trafficking.* Curr Biol, 2013. **23**(13): p. 1173-80.
25. Sönnichsen, B., et al., *Distinct Membrane Domains on Endosomes in the Recycling Pathway Visualized by Multicolor Imaging of Rab4, Rab5, and Rab11.* Journal of Cell Biology, 2000. **149**(4): p. 901-914.
26. Rai, A., et al., *Dynein Clusters into Lipid Microdomains on Phagosomes to Drive Rapid Transport toward Lysosomes.* Cell, 2016. **164**(4): p. 722-734.
27. Pfeffer, S., *Membrane Domains in the Secretory and Endocytic Pathways.* Cell, 2003. **112**(4): p. 507-517.
28. Franke, C., et al., *Correlative single-molecule localization microscopy and electron tomography reveals endosome nanoscale domains.* Traffic, 2019. **20**(8): p. 601-617.
29. Picas, L., et al., *BIN1/M-Amphiphysin2 induces clustering of phosphoinositides to recruit its downstream partner dynamin.* Nat Commun, 2014. **5**: p. 5647.
30. Chudakov, D.M., S. Lukyanov, and K.A. Lukyanov, *Using photoactivatable fluorescent protein Dendra2 to track protein movement.* Biotechniques, 2007. **42**(5): p. 553, 555, 557 passim.
31. Culley, S., et al., *SRRF: Universal live-cell super-resolution microscopy.* The international journal of biochemistry & cell biology, 2018. **101**: p. 74-79.
32. Lawe, D.C., et al., *Sequential roles for phosphatidylinositol 3-phosphate and Rab5 in tethering and fusion of early endosomes via their interaction with EEA1.* J Biol Chem, 2002. **277**(10): p. 8611-7.
33. Lawe, D.C., et al., *The FYVE domain of early endosome antigen 1 is required for both phosphatidylinositol 3-phosphate and Rab5 binding. Critical role of this dual interaction for endosomal localization.* J Biol Chem, 2000. **275**(5): p. 3699-705.
34. Rubino, M., et al., *Selective membrane recruitment of EEA1 suggests a role in directional transport of clathrin-coated vesicles to early endosomes.* J Biol Chem, 2000. **275**(6): p. 3745-8.
35. Mishra, A., et al., *Structural basis for Rab GTPase recognition and endosome tethering by the C2H2 zinc finger of Early Endosomal Autoantigen 1 (EEA1).* Proceedings of the National Academy of Sciences of the United States of America, 2010. **107**(24): p. 10866-10871.
36. Larsen, A.H., et al., *Membrane-binding mechanism of the EEA1 FYVE domain revealed by multi-scale molecular dynamics simulations.* PLOS Computational Biology, 2021. **17**(9): p. e1008807.
37. Merithew, E., et al., *Determinants of Rab5 Interaction with the N Terminus of Early Endosome Antigen 1 *.* Journal of Biological Chemistry, 2003. **278**(10): p. 8494-8500.
38. Lawe, D.C., et al., *Essential role of Ca2+/Calmodulin in Early Endosome Antigen-1 Localization.* Molecular Biology of the Cell, 2003. **14**(7): p. 2935-2945.
39. Mills, I.G., S. Urbé, and M.J. Clague, *Relationships between EEA1 binding partners and their role in endosome fusion.* J Cell Sci, 2001. **114**(Pt 10): p. 1959-65.
40. Wang, H., et al., *Phosphatidylinositol 3,4-bisphosphate synthesis and turnover are spatially segregated in the endocytic pathway.* The Journal of biological chemistry, 2020. **295**(4): p. 1091-1104.
41. Perini, E.D., et al., *Mammalian CORVET Is Required for Fusion and Conversion of Distinct Early Endosome Subpopulations.* Traffic, 2014. **15**(12): p. 1366-1389.
42. Di Guglielmo, G.M., et al., *Distinct endocytic pathways regulate TGF-beta receptor signalling and turnover.* Nat Cell Biol, 2003. **5**(5): p. 410-21.
43. Grimes, M.L., et al., *Endocytosis of Activated TrkA: Evidence that Nerve Growth Factor Induces Formation of Signaling Endosomes.* The Journal of Neuroscience, 1996. **16**(24): p. 7950.
44. Wiley, H.S. and P.M. Burke, *Regulation of Receptor Tyrosine Kinase Signaling by Endocytic Trafficking.* Traffic, 2001. **2**(1): p. 12-18.
45. Wang, Y., et al., *Endosomal signaling of epidermal growth factor receptor stimulates signal transduction pathways leading to cell survival.* Molecular and cellular biology, 2002. **22**(20): p. 7279-7290.

46. Fürthauer, M. and M. González-Gaitán, *Endocytic Regulation of Notch Signalling During Development.* Traffic, 2009. **10**(7): p. 792-802.
47. Irannejad, R., et al., *Conformational biosensors reveal GPCR signalling from endosomes.* Nature, 2013. **495**(7442): p. 534-8.
48. Stanoev, A., et al., *Interdependence between EGFR and Phosphatases Spatially Established by Vesicular Dynamics Generates a Growth Factor Sensing and Responding Network.* Cell Syst, 2018. **7**(3): p. 295-309.e11.
49. Sorkin, A. and M. von Zastrow, *Endocytosis and signalling: intertwining molecular networks.* Nat Rev Mol Cell Biol, 2009. **10**(9): p. 609-22.
50. Scita, G. and P.P. Di Fiore, *The endocytic matrix.* Nature, 2010. **463**(7280): p. 464-473.
51. Villaseñor, R., Y. Kalaidzidis, and M. Zerial, *Signal processing by the endosomal system.* Curr Opin Cell Biol, 2016. **39**: p. 53-60.
52. Howe, C.L., *Modeling the signaling endosome hypothesis: why a drive to the nucleus is better than a (random) walk.* Theoretical biology & medical modelling, 2005. **2**: p. 43-43.
53. York, H.M., et al., *Rapid whole cell imaging reveals a calcium-APPL1-dynein nexus that regulates cohort trafficking of stimulated EGF receptors.* Communications Biology, 2021. **4**(1): p. 224.
54. Vonderheit, A. and A. Helenius, *Rab7 associates with early endosomes to mediate sorting and transport of Semliki forest virus to late endosomes.* PLoS biology, 2005. **3**(7): p. e233-e233.
55. Laine, R.F., et al., *NanoJ: a high-performance open-source super-resolution microscopy toolbox.* Journal of Physics D: Applied Physics, 2019. **52**(16): p. 163001.
56. El Beheiry, M. and M. Dahan, *ViSP: representing single-particle localizations in three dimensions.* Nat Methods, 2013. **10**(8): p. 689-90.